Human immunodeficiency virus type 2 capsid protein mutagenesis defines the determinants for Gag-Gag interactions

Huixin Yang[1,4], Nathaniel Talledge[1,2,3], William E. Arndt[1,2,5], Wei Zhang[1,2,6]* and Louis M. Mansky[1,2,3,4,5,6]*

[1] Institute for Molecular Virology, University of Minnesota – Twin Cities, Minneapolis, MN 55455 USA

[2] Division of Basic Sciences, School of Dentistry, University of Minnesota – Twin Cities, Minneapolis, MN 55455 USA

[3] Masonic Cancer Center, University of Minnesota – Twin Cities, Minneapolis, MN 55455 USA

[4] Comparative Molecular Biosciences Graduate Program, University of Minnesota – Twin Cities, St. Paul, MN 55108, USA.

[5] Biochemistry, Molecular Biology & Biophysics Graduate Program, University of Minnesota – Twin Cities, Minneapolis, MN 55455 USA

[6] Characterization Facility, College of Sciences and Engineering, University of Minnesota – Twin Cities, Minneapolis, MN 55455 USA

* Corresponding authors: mansky@umn.edu, zhangwei@umn.edu

Abstract

Human immunodeficiency virus (HIV) Gag drives particle assembly. The capsid (CA) domain is critical for Gag oligomerization, and encodes key residues that dictate Gag-Gag interactions and particle morphology. The immature particle morphology of HIV-2 is intriguing different relative to that of HIV-1. To help define the critical determinants for Gag-Gag interactions and investigate the differences between HIV-1 and HIV-2, we have conducted mutagenesis in targeted locations of HIV-2 CA that have been implicated in Gag-Gag interactions. In particular, a panel of 31 site-directed mutants at the HIV-2 CA inter-hexamer interface, intra-hexamer interface and CA inter-domain linker have been created and analyzed for the efficiency of particle production, particle morphology, particle infectivity, Gag subcellular distribution and *in vitro* protein assembly. Seven conserved residues (L19A, A41, I152, K153, K157, N194, D196) and two non-conserved residues (G38, N127) were found that impact Gag multimerization and particle assembly. Taken together, these observations complement structural analyses of immature HIV-2 particle morphology and Gag lattice organization, and provide insights into the morphological differences between HIV-1 and HIV-2 immature particles and their impact on virus replication.

Introduction

Human immunodeficiency virus (HIV) belongs to the genus *Lentivirus,* the family *Retroviridae*. To date, HIV has infected more than 70 million people worldwide [1]. HIV has two main types, HIV-1 and HIV-2, which have similarities in life cycles, transmission modes, and clinical consequences [2]. Despite these similarities there are differences in the prevalence, transmission rate, and infectivity of these two viruses. Compared to HIV-1, HIV-2 is less widespread and less infective [2, 3]. HIV-2 also has lower viral loads during the course of the infection, slower rates of CD4 decline, and delayed clinical progression [4]. HIV-2 patients are considered less infectious in the early stages of infection and long-term nonprogressors [5, 6]. The different steps of the HIV life cycle are targeted by combined antiretroviral therapy (ART) drugs, leading to a remarkable reduction in overall morbidity and mortality [10, 11].

The HIV assembly pathway is an underdeveloped target for the discovery and advancement of antiretroviral drugs, so our studies focused on this step. Although much effort has been undertaken to target the assembly of HIV particles [7-11], none of these efforts to date have resulted in an approved anti-HIV drug. HIV capsid (CA) is a promising antiviral drug target, because its stability and integrity are critical to the normal life cycle and infectivity of the virus [12]. For instance, Lenacapavir (LEN, GS-6207, GS-CA2), a long-acting HIV-1 CA inhibitor, currently in phase 2/3 clinical trials, sought FDA approval [13]. LEN binds to he hydrophobic pocket formed by two adjoining CA subunits within the hexamer. Meanwhile, HIV-2 is has been shown to be resistant to effective anti HIV-1 drugs [14, 15]. Therefore, it is critical to investigate the molecular difference between HIV-1 and HIV-2 to develop effective treatments for both virus types.

HIV Gag protein is the essential structural protein responsible for orchestrating the majority of steps in HIV assembly [11]. HIV Gag has a low level (59% identity, 72% similarity) of amino acid sequence conservation between HIV-1 (NL4-3) and HIV-2 (ROD) strains. Most assembly steps are performed by three Gag subdomains. Matrix (MA) is responsible for Gag-membrane binding [16, 17]. Nucleocapsid (NC) interacts with the viral RNA packaging signal and encapsidates the viral genome [18]. CA is critical for Gag oligomerization during virus assembly and core formation during virus maturation and is divided into two structurally distinct domains, CA_{NTD} and CA_{CTD} [19], which are connected by a flexible inter-domain linker. The major homology region (MHR), a 20-residue segment (residues HIV-1 CA 153-172) toward the N-terminus of CA_{CTD}, is highly conserved. During particle assembly, Gag polyproteins ($Pr55^{Gag}$) initially accumulate at the plasma membrane forming a radially arranged lattice that curves and deforms the membrane [16]. The accumulated Gag drives budding and release forming an

immature virus particles. Then, HIV protease (PR) cleaves the Gag polyprotein into each of the respective domains to form a mature particle [20]. In the center of the particle, CA reassembles into a cone-shaped core which contains a dimeric viral genomic RNA associated with NC [16].

The morphologies of HIV-1 immature and mature particles have been well studied [21, 22]. Previous studies showed that the overall mature HIV-1 particle is made from a lattice of ~250 CA hexamers closed by the insertion of 12 CA pentamers [23]. However, there is no pentamers in the immature HIV-1 Gag lattice since the pentamers mediate areas of high curvature of the mature conical core that is not present in the immature lattice. The CA hexamer contains an inner ring of six CA NTDs held together by contacts between adjacent CA molecules [24, 25]. The interactions between CA monomers are related by 6-fold symmetry within a hexamer (intra-hexamer) and by 3-fold and 2-fold symmetry between neighboring hexamers (inter-hexamer). The hexamers are stabilized by interactions at these interfaces [23].

To date, surprising and intriguing differences have been discovered between the immature Gag lattice structure of HIV-1 and other retroviruses, although HIV-1 and HIV-2 CA have a moderate level of amino acid sequence conservation (69% identity, 80% similarity, **Fig. 1A**). Moreover, many immature Gag lattice structures have been published, such as Rous sarcoma virus (RSV) [26], Murine leukemia virus (MLV) [27], and HIV-1 [28]. Given previous observations that specific amino acid residues in Gag CA encode the key determinants that dictate virus particle morphology, we hypothesized that the differences between HIV-1 and HIV-2 Gag CA lead to differences in viral assembly and ultimately infectivity. We also investigated what HIV-2 CA-CA interactions were critical for virus particle assembly and explained why the critical residues are responsible for various HIV-2 phenotypes.

Critical amino acid residues in CA dictate virus particle morphology. Mutagenesis studies confirmed the importance of interface residues for core morphology and stability and virion infectivity [23, 24, 29, 30]. Mutations in the CA have been shown to affect particle assembly and virion infectivity in different retroviruses, such as HIV-1 [31], Simian immunodeficiency virus (SIVmac) [32], Mason-Pfizer monkey virus (M-PMV) [33], and RSV [34]. Several key mutants, such as HIV-1 CA W184A and M185A caused Gag assembly defects, produced non-infectious viruses, reduced CA dimerization and intermolecular Gag–Gag interactions *in vitro*, diminished immature particle production *in vivo*, and abolished CA dimerization [29, 35]. Moreover, parallel studies have been done on SIVmac constructs [32]. However, there have been no studies focused on HIV-2 critical amino acids. We hypothesized that the mutants at HIV-2 Gag CA inter- and intra-hexameric interfaces result in inefficient particle assembly.

A previous study investigating HIV-1 and SIVmac residues swaps examined the mutant effects on particle infectivity and production [36]. Select mutations in HIV-1 CA Helix 7, such as E128N, I141C, were found less infectivity and reduced more than 50% particle production when swapped to the corresponding SIVmac residue [36]. This indicated that some non-conserved amino acids in HIV-1 CA Helix 7 showed important functions.

To investigate the differences between HIV-1 and HIV-2, a panel of 10 site-directed mutants in non-conserved HIV-2 CA residues based on sequence alignment with HIV-1 **(Fig. 1A)** was also conducted by mutating HIV-2 CA residues to HIV-1 types to analyze the efficiency of immature particle production and Gag subcellular distribution. None of the ten mutants were previously tested in HIV-2 studies, and eight mutants (except N127E and C140I) were not examined in either HIV types. Of the conserved residue swaps none of the HIV-2 CA mutations were previously reported, and four mutations (L19A, I152A, K153A, N194A) were unique to both HIV-1 and HIV-2. Selected mutants were additionally analyzed for mature particle production, infectivity, Gag subcellular distribution and *in vitro* protein assembly. HIV-2 critical residues and novel CA-CA interactions were discovered.

These efforts provided the mechanistic detail of CA residues that mediate viral particle assembly, and highlight fundamental differences between HIV-1 and HIV-2 CA. Our studies also provided further insight into the fundamental aspects of HIV particle assembly that will inform efforts to discover new antiretroviral drug targets for HIV therapies.

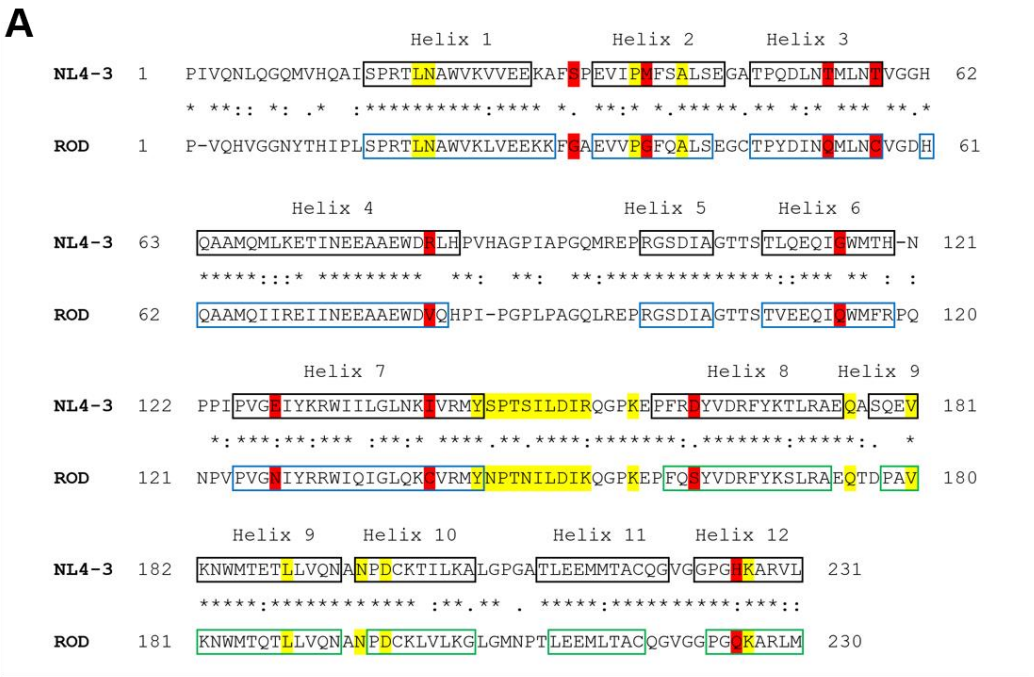

Fig 1A. Alignment of HIV-1 and HIV-2 CA sequences. Amino acid sequences in CA of HIV-1 NL4-3 (GenBank accession no. AF324493; CA 1-231; Gag 133-363) and HIV-2 ROD (GenBank accession no. M15390; CA 1- 230; Gag 136-365) were aligned by Clustal Omega Multiple Sequence Alignment [1]. Locations of HIV-1 immature CA helices in this alignment are as described previously [2] (PDB ID: 5L93) and indicates by black boxes. HIV-2 immature CA_{NTD} (CA aa, 1-144; Gag aa, 136-279) helices are as described previously [3] (PDB ID: 2WLV), and indicates with blue boxes. CA_{CTD} (CA aa,145-230; Gag aa, 280-365) helices are predicted by the PSIPRED server [4, 5], indicates by green boxes. "*" indicates conserved amino acids; ":" indicates amino acid substitution with high amino acid similarity; "." indicates amino acid substitutions with low similarity. Yellow highlight indicates alanine-scanning mutagenesis on conserved residues. Red highlight indicates mutagenesis on non-conserved residues, which HIV-2 residues were mutated to HIV-1 types. **(B) Structure of CA hexamer.** Mutagenesis of conserved residues were colored yellow, and mutagenesis of non-conserved residues were colored red. **(C) Structure of CA monomer.**

Results

Mutations to conserved CA residues decrease immature particle production

Given previous observations that specific amino acid residues in Gag CA encode the key determinants that dictated virus particle morphology, CA-CA interactions for a multitude of retroviruses such as HIV-1, MLV, and RSV [26-28, 37, 38]. However, there were few mutants of HIV-2 Gag CA residues have been demonstrated to inhibit particle assembly. To identify critical residues in HIV-2 Gag CA that mediate HIV particle assembly with detailed molecular analysis we conducted an exhaustive search of comparative analysis between previous studies in HIV-1 and HIV-2 [29, 35, 39]. First, we conducted alanine-scanning mutagenesis in targeted locations of the CA protein that have been implicated in encoding critical amino acid residues important for CA-CA interactions that impact virus particle assembly and release from cells. In particular, a panel of twenty-one mutants was created and analyzed for the efficiency of particle production through immunoblot detection and quantification of Gag protein products in an HIV-2 tractable virus-like particle (VLP) model system validated to mimic authentic immature virus particle assembly and release closely (**Fig. 2**).

We conducted ten site-directed mutants at the HIV-2 CA_{NTD}-CA_{CTD} linker domain (**Fig. 2A**). Two mutations I152A and K153A were discovered to reduce immature particle production significantly, 3.9-fold, and 4-fold relative to WT levels, respectively as assessed by p24 levels in immunoblots of viral supernatants (**Fig. 2A**). These two mutants are in the MHR region. The previous publication has reported that some conserved HIV-1 MHR residue substitution (i.e., HIV-1 Q155N) leads to a dramatic reduction in immature particle production in human and nonhuman primate cells expressing HIV-1 proviruses [40]. Moreover, I152A was a novel mutant that the parallel mutant (HIV-1 I153A) had not been generated in HIV-1.

Five site-directed mutants were conducted at the intra-hexamer interface, four of them (L19A, K157A, N194A, and D196A) produced at least 2-fold less immature particles than HIV-2 WT (**Fig. 2B**). L19A and N194A were novel mutants that have not been tested in HIV-1 CA, produced 3.5-fold and 4.5-fold less immature particles than WT, respectively. K157A and D196A, which produced 2.1-fold and 2.8-fold less immature particles, respectively, were reported reduced particle production in HIV-1 CA [29, 35, 41].

Four site-directed mutants at the 2-fold inter-hexamer interface and two mutants at 3-fold inter-hexamer interface were selected to analyze relative immature particle production (**Fig. 2C**). All 2-fold inter-hexamer interface showed similar immature particle production to HIV-2 WT except N20A which had a modest decrease in production (~92% of WT). One of two mutants at

3-fold inter-hexamer interface, A41D, significantly reduced immature particle production by 4.6-fold (**Fig. 2C**).

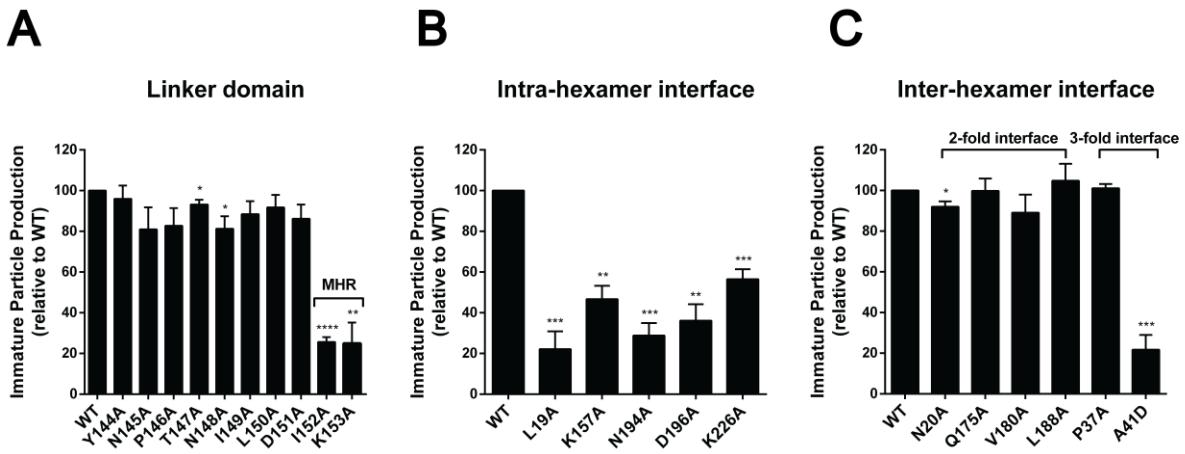

Fig 2. Relative immature particle production of HIV-2 CA mutants at CA_{NTD}-CA_{CTD} linker (A), intra-hexamer interface (B), and inter-hexamer interface (C). 293T/17 cells were transfected with untagged HIV-2 Gag expression constructs (WT or alanine-scanning mutants), and the cell culture supernatants were harvested 48h post transfection. Immunoblot analysis was conducted to determine the amount of immature particle production for WT and CA conserved mutants. The relative particle production of CA mutants was calculated relative to WT. Histograms are presented to indicate the relative immature particle production of HIV-2 CA alanine-scanning mutants. Error bars represent standard error of the mean from three independent experiments. Significance relative to WT was determined by unpaired t test. ****, $P < 0.0001$; ***, $P < 0.001$; **, $P < 0.01$; *, $P < 0.05$. MHR = Major homology region.

Mutations to non-conserved CA residues decrease immature particle production

Preliminary data has discovered striking morphological differences between immature HIV-1 and HIV-2 particles that argue in support of a model in which relatively minor changes in the geometry of protein-protein interactions can profoundly impact overall particle morphology [3]. To investigate the differences between HIV-1 and HIV-2 CA, a panel of 10 site-directed mutants in non-conserved HIV-2 CA residues was conducted by mutating HIV-2 CA residues to the HIV-1 residue equivalent from the CA sequence alignment (**Fig. 1 and Fig. 3**). Two mutants HIV-2 CA mutants (G38M and N127E) were discovered to produce less than 50% of WT immature particles. Both of these residues are located at the 3-fold inter-hexamer interface in the CA_{NTD} based on structural comparisons to HIV-1 lattice structures.

HIV-2 G38M showed reductions in immature and mature particle production, which are 2.7-fold (**Fig. 3A**) and 2-fold less than WT (**Fig. 4C**), respectively. HIV-1 M39G mutant was also generated to test mature HIV-1 particle production, resulting in 2.6-fold less particle production than WT (**Fig. 4A**).

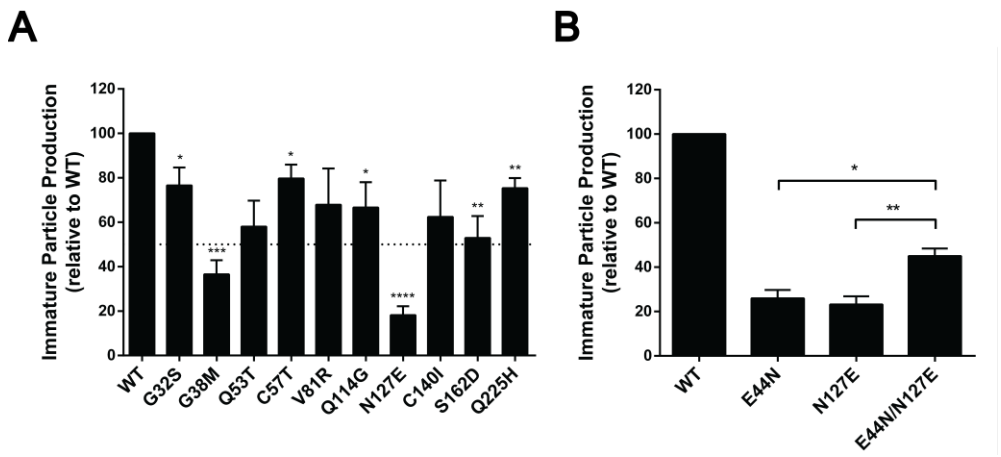

Fig 3. Relative immature particle production for a panel of HIV-2 CA mutants on non-conserved residues. (A) Relative immature production of HIV-2 non-conserved residue mutants. (B) Relative immature particle production of HIV-2 CA E44N, N127E and E44N/N127E. 293T/17 cells were transfected with untagged HIV-2 Gag expression constructs (WT or mutants), and the cell culture supernatants were harvested 48h post transfection. Immunoblot analysis was conducted to determine the amount of particle production for WT and mutants. The relative immature particle production of CA mutants were calculated relative to WT. Histograms are presented to indicate the relative particle production of HIV-2 CA mutants. Error bars represent standard error of the mean from three independent experiments. Significance relative to WT was determined by unpaired t test. ****, $P < 0.0001$; ***, $P < 0.001$; **, $P < 0.01$; *, $P < 0.05$.

In a previous study, E128 residue was mutated to the corresponding HIV-2 residue (HIV-1 E128N) and found to decrease viral replication [36]. HIV-2 N127E immature particle production is 4.3-fold less than WT (**Fig. 3A**), and mature particle production is 6.7-fold less than WT (**Fig. 4C**). HIV-1 E128N mature particle production in our studies is 2.6-fold less than WT. Investigating the position of E128 in the HIV-1 immature CA cryo-EM structure [21] indicates that E128 is within interaction distance (<4 Å) with E45. Based on the HIV-2 sequence, two single mutations (HIV-2 E44N, N127E) were generated to compare with WT (E44/N127). The immature particle production of two single mutations, E44N and N127E, was about 4-fold less than the WT, (**Fig. 3B**). To assess if these two residues positions in HIV-2 are interacting we performed the double mutation E44N/N127E in the HIV-2 backbone. The immature particle production showed a ~2-fold increase from either of the single mutants, but was 2-fold less than WT.

Mutations perturb normal Gag subcellular distribution

Gag subcellular distribution is one of the most critical environmental factors contributing to Gag oligomerization [16]. To investigate the subcellular distribution of HIV-2 mutant Gag compared to WT, select mutants were analyzed due to significant reduction of immature particle production. This mutants were L19A at the intra-hexamer interface, A42D at the inter-hexamer interface, I152A at the CA_{NTD}-CA_{CTD} linker domain, non-conserved G38M and N127E. Then, the HIV-2 WT and mutant Gag-YFP constructs were transfected into Hela cells. HIV-2 WT Gag

proteins were localized to the plasma membrane as well as in the cytoplasm in a characteristic punctate distribution pattern, indicative of Gag oligomerization, as described in previous studies [38]. Among these five mutants, cells transiently transfected with HIV-2 G38M and N127E Gag-YFP showed a diffuse fluorescence localization in the cytoplasm along with enrichment within or immediately surrounding the nucleus (**Fig. 5**). These observations suggested that G38M and N127E perturb the normal subcellular localization of Gag. HIV-2 G38M and N127E are non-conserved residues in the 3-fold interface and indicated that G38 and N127 play an role in HIV-2 Gag subcellular distribution.

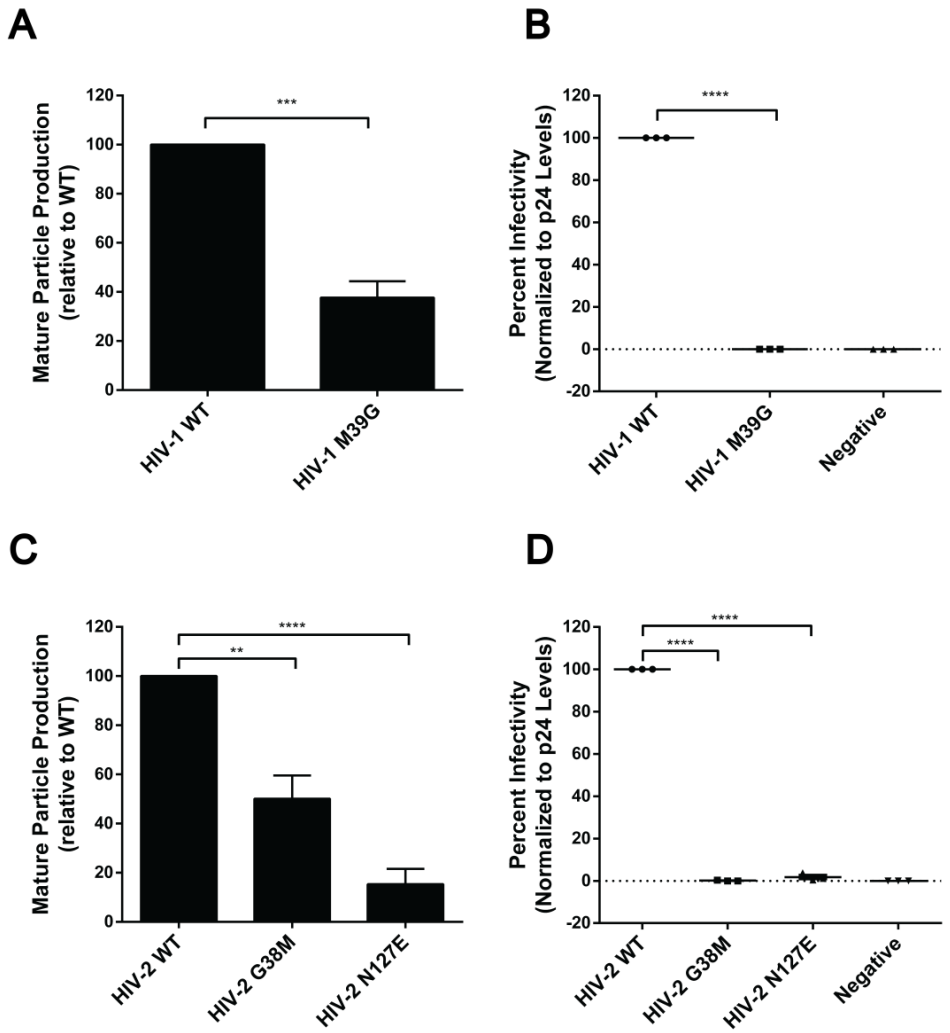

Fig 4. Relative mature particle production and infectivity analysis. 293T/17 cells were transfected with HIV-1 NL43 MIG (A,B) or HIV-2 ROD MIG (C,D) constructs (WT or mutants) and VSVG, and the mature particles were harvested from the cell culture supernatants. (A,C) Relative mature particle production. Immunoblot analysis was conducted to determine the amount of particle production for WT and mutants. HIV CA was evaluated by detection with an StarBright™ Blue 700 secondary antibody. (B,D) Relative infectivity. MAGI cells were then challenged with HIV MIG-VSVG viral supernatants or fresh medium (Negative control) and collected 48 h postinfection. Infectivity was determined by flow cytometry analysis for expression of GFP and mCherry, which are both encoded by the vectors. Relative infectivity was determined and normalized to particle production. Error bars represent standard deviations

from three independent experiments. Significance relative to WT was determined by unpaired t test. ****, $P < 0.0001$; ***, $P < 0.001$; **, $P < 0.01$.

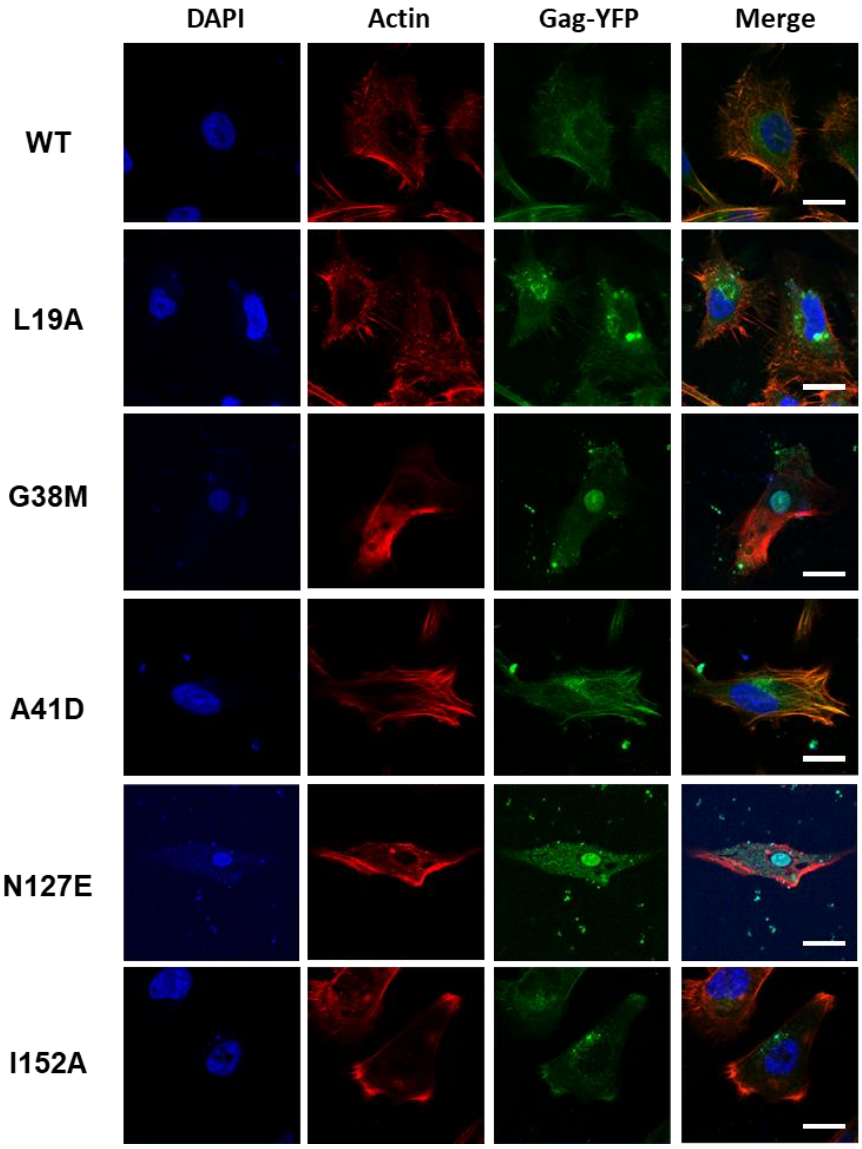

Fig 5. Subcellular distribution of HIV-2 Gag for CA mutants. HeLa cells were transfected with a WT HIV-2 Gag-eYFP or the indicated mutant Gag. Representative images for WT HIV-2 Gag-eYFP and for the mutants L19A, G38M, A41D, N127E and I152A are shown. At least 15 individual cells were imaged across three independent replicates for a total of 15 cells. Scale bar, 20 μm

G38M and N127E disrupt HIV-2 immature particle morphology

Generally, the knowledge of critical residues of HIV-2 CA that dictate particle morphology is limited as compared to other retroviral genera. However, previous studies have discovered surprising and intriguing differences between the immature Gag lattice structure of HIV-1 and other retroviruses [26-28, 37]. Preliminary data in our lab also discovered striking morphological

differences between immature WT HIV-1 and HIV-2 particles that argue in support of a model in which relatively minor changes (such as site-directed mutagenesis) in the geometry of protein-protein interactions can have a profound impact on overall particle morphology [38].

Two key mutants, G38M and N127E, which significantly reduced the immature and mature particle production, and had a unique Gag subcellular distribution phenotypes, were selected and the immature particle morphology was examined. HIV-2 WT immature particles had a uniform particle morphology similar to the previous observations [38] (**Fig. 6A**). In particular, HIV-2 WT immature particles had a very organized CA lattice beneath the viral membrane. This organized density suggested a tightly packed immature Gag lattice closely following the inner viral membrane. The majority of the HIV-2 WT immature particles were discovered to be spherical, with small portion of the population showing other morphologies (**Fig. 6A**). However, approximately 25% of HIV-2 G38M (**Fig. 6B**) and N127E (**Fig. 6C**) immature particles have non-spherical morphologies, such as droplet, angular, and peanut shapes. Unlikely WT, most G38M and N127E immature particles did not show a organized CA lattice beneath the lipid bilayer, suggesting incomplete or disorganized Gag lattices in the particles. These observations suggested that the G38M and N127E mutants possess a defect in the ability of Gag to oligomerize and form a defined lattice structure, which is a requisite step for infectious particle formation.

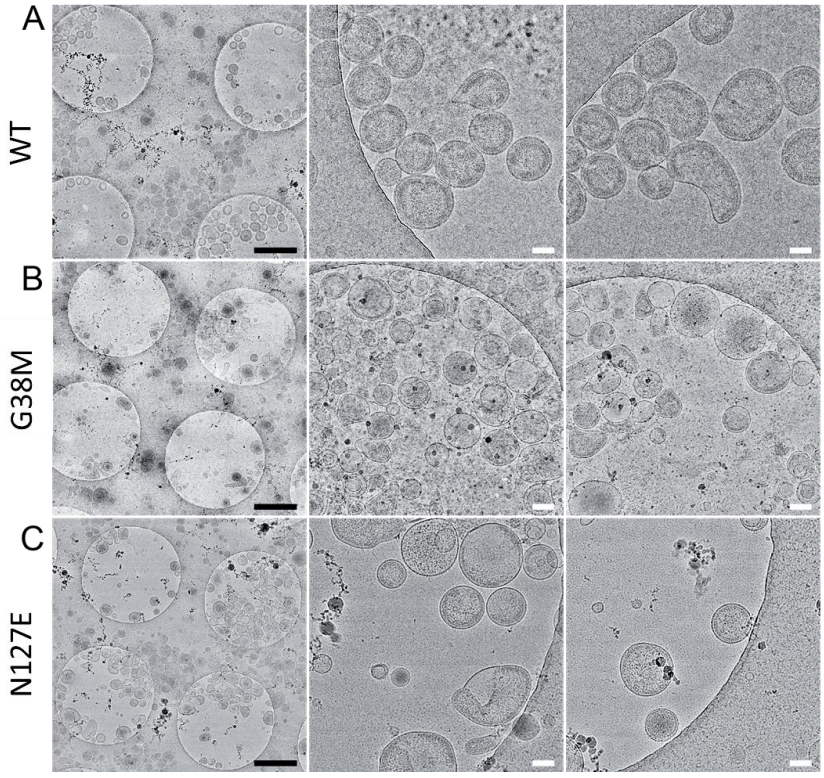

Fig 6. Cryo-EM images of VLPs produced by selected CA mutants. 293T/17 cells were transfected with untagged HIV-2 Gag expression constructs (WT or selected mutants), and the immature particles were concentrated and purified from cell culture supernatants prior to cryo-EM analysis. Shown are representative images of CA mutants with two magnifications. At least 200 particles were imaged per mutant. Black scale bars, 1 um; white scale bars, 100 nm.

G38M and N127E significantly decrease HIV-2 particle infectivity

Infectivity assays of CA point mutants provided robust evidence that a single amino acid change might disrupt Gag-Gag interactions that impact the HIV life cycle. A single-cycle infectivity system with a fluorescent reporter system was used as previously described [42]. HIV pseudoviruses were collected and MAGI cells were challenged with WT or select CA mutant harboring virions. After 48 hours, the MAGI cells were collected and examined via flow cytometry. Relative infectivity was determined and normalized to mature particle production levels by Gag detection in viral supernatants.

HIV-2 G38M and N127E were selected for the infectivity assay and exhibited a remarkably decreased viral infectivity compared to WT, which infectivity was reduced more than 100-fold and 56-fold less than WT, respectively (**Fig. 4D**). To assess if the equivalent mutations in HIV-1 (see **Fig. 1A**) have similar impacts on particle infectivity, the site-direct mutant HIV-1 CA M39G mutant exhibited single-cycle infectivity rates xxx fold reduced from WT and HIV-1 CA N128E from a previous HIV-1 study reported 50-fold less than WT [36].

Mutations disrupt HIV-2 CA-NC assembly *in vitro*

In vitro protein assembly is commonly used for analyzing Gag-Gag interactions as it's an efficient system to specifically perturb CA interactions and separate it from other cellular effects [43]. To assess the effects of select HIV-2 CA mutations on CA-CA interactions an HIV-2 CA-NC protein construct was purified from *E. coli* to conduct *in vitro* assembly assays (see methods). The purified proteins were dialyzed against assembly buffer conditions that induce helical assemblies to form with WT HIV-2 CA-NC protein and then quantified by measuring the reaction turbidity at A340 nm. We used a previously established model that the turbidity of the solution reflected the status of protein assembly [44, 45]. The assemblies for WT and five HIV-2 CA mutants (L19A, G38M, A41D, N127E, and I152A) were monitored with turbidity measurements every 20 minutes for 2 hours and corrected for any changes in reaction volume due to dialysis **(Fig. 7**). Due to the significant reduction of immature particles, L19A at the intra-hexamer interface (**Fig. 7B**), A42D at the inter-hexamer interface (**Fig. 7D**), I152A at the CA_{NTD}-CA_{CTD} linker domain (**Fig. 7F**), non-conserved G38M (**Fig. 7C**) and N127E (**Fig. 7E**) were chosen for HIV-2 CA-NC assembly assay.

The normalized 340 nm value of HIV-2 WT (**Fig. 7A**) peaked at 20 min at 1.27, then slowly decreased and remained stable at 0.56. HIV-2 L19A (**Fig. 7B**), G38M (**Fig. 7C**), and I152A (**Fig. 7F**) had similar trends with WT (**Fig. 7A**), but with normalized A340 nm values 1.77, 0.34, and 0.65, respectively. N127E reached a peak at 40 min, with an A340 nm value of 0.36 (**Fig. 7E**). A41D showed low turbidity readings during the experimental time course, of which A340 nm value was always less than 0.03 (**Fig. 7D**). G38M, A41D, N127E and I152A showed decreased assembly kinetics compared to WT.

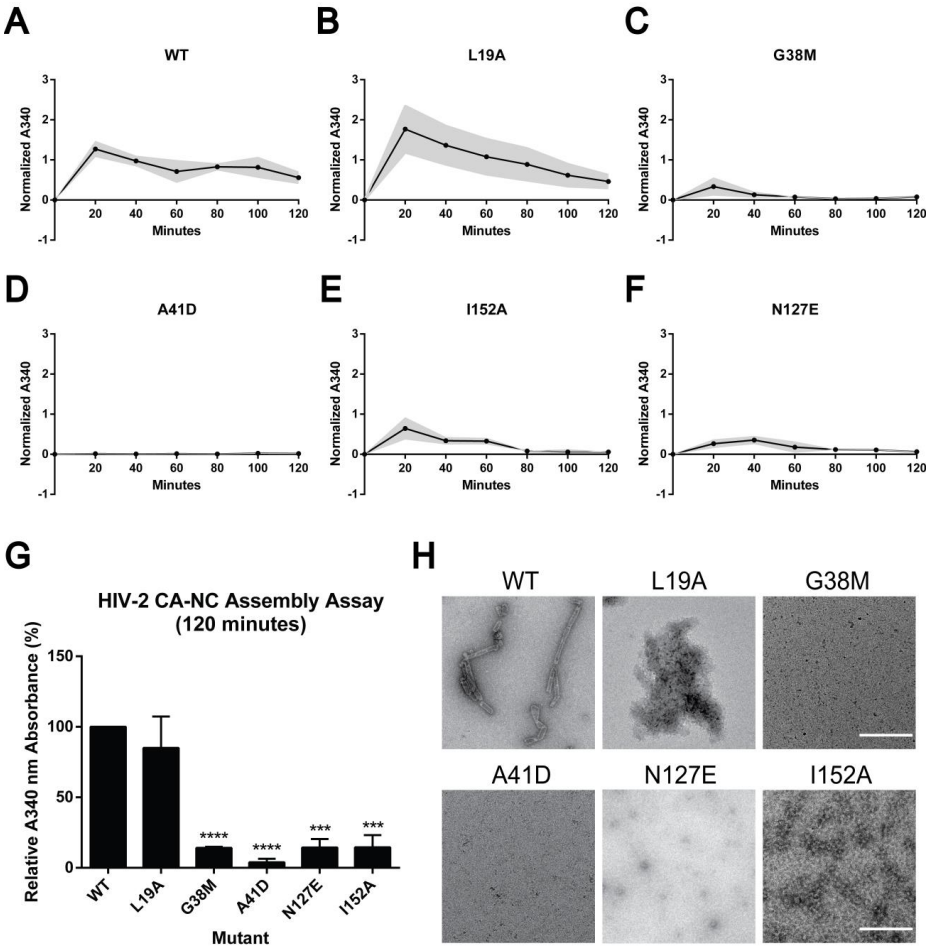

Fig 7. *In vitro* HIV-2 CA-NC assembly analysis. (A-F) Assembly kinetics of HIV-2 WT and selected mutants were monitored by measuring light scattering at 340 nm while dialyzing the reaction from sizing buffer into the assembly buffer at the indicated times. Readings were taken every 20 minutes for 2 hours and corrected for any changes in reaction volume due to dialysis. The grey area represents average ± standard error of the mean from three independent experiments. (G) Relative A340 nm absorbance of selected HIV-2 CA mutants to WT, sampled at 120 minutes. Error bars represent standard error of the mean from three independent experiments. Significance relative to WT was determined by unpaired t test. ****, $P < 0.0001$; ***, $P < 0.001$. (H) Negative staining EM images of assembly products, sampled at 120 minutes. Scale bar, 500 nm.

At the final endpoint (120 minutes), G38M, A41D, N127E, and I152A showed significant reductions of relative A340 nm values compared to WT, which were 7.0-fold, 25.6-fold, 6.9-fold,

6.9-fold less than WT, respectively (**Fig. 7G**). These observations indicated that these mutants form unstable assembly products that disrupted the CA-NC helical assembly. However, L19A did not show a significant reduction in relative A340. These observations indicated that mutants, except L19A, had assembly defects. These residues play critical roles in *in vitro* protein assembly. Similar to HIV-2 A42D having 25.6-fold less than WT, HIV-1 A42D CA-NC protein assembly was impaired, and assembled CA-NC particles were 20-fold less than WT [43].

Then the assembly products were visualized by negative stain TEM. HIV-2 WT CA-NC assembled into stable, regularly ordered uniform tubular structures, while G38M, A41D, N127E, and I152A did not show protein assemble products (**Fig. 7H**). L19A CA-NC showed protein aggregations without uniform tubular structures formed, suggesting that the observed turbidity signal was due to large protein aggregates versus ordered helical tubes. These results indicate all selected mutants had defects in CA-CA interactions that prevented helical tube formation *in vitro.*

Discussion

Particle morphologies among retroviral genera are quite distinct, with intriguing differences observed relative to HIV-1. Intriguingly, HIV-2 produces immature particles distinct from HIV-1 – *i.e.,* they possess a nearly complete immature Gag lattice, have a larger than average particle diameter, and have a higher average copy number of incorporated Gag. However, to our knowledge, this is the first time a panel of HIV-2 mutagenesis was created to analyze HIV-2 Gag-Gag interactions.

The two primary goals of our experiments were: (i) to investigate the critical role of the HIV-2 CA for Gag-Gag interactions and virus particle assembly; (ii) to identify the difference between HIV-1 and HIV-2 CA that alter particle assembly properites. In the study, we created two panels of site-directed mutants to achieve these goals **(Fig. 1)**. One panel of 21 alanine-scanning site-directed mutants in HIV-2 CA conserved residues, and another panel of 10 mutants at non-conserved residues by swapping the native HIV-2 residues to the residues from HIV-1 CA.

We interrogated key residues in HIV-2 CA, and these mutants are located on CA intra-hexamer interface, inter-hexamer interface, and linker domain. The specific residues were chosen for mutagenesis based on structural comparisons between HIV-1 and HIV-2 CA, and previous publications in HIV-1 [29, 35, 36, 43, 46]. To indicate a disruption of productive Gag-Gag interactions with the select mutant we set a criteria of a two-fold decrease in particle production for further investigation. The majority of mutants had no overall effect on immature particle production, seven conserved mutants (L19A, A41D, I152A, K153A, K157A, N194A, D196A) and two non-conserved mutants (G38M, N127E) were found to impact Gag-Gag interactions based on our selection criteria **(Fig. 2 and Fig. 3)**.

For the mutants in conserved residues, the mutants at the HIV-2 CA_{NTD}-CA_{CTD} linker domain did not significantly reduce immature particle production unless they were at the MHR domain **(Fig. 2A)**. Mutants at the intra-hexamer interface reduced particle production **(Fig. 2B).** Additionally, mutants in the 3-fold interface but not the 2-fold interface significantly reduced particle production **(Fig. 2C)**. These observations indicated that the residues at the intra-hexamer interface and 3-fold inter-hexamer interface are critical for immature particle production and CA-CA interactions. Some key residues, such as L19, I152 and N194, were not identified in HIV studies.

We discovered two key mutants (G38M and N127E) in non-conserved residues, which showed intriguing observations. The key features of the HIV-2 CA G38M and N127E were a significant reduction of immature particle production **(Fig. 3)** and a significant reduction of mature particle production. This indicates that these mutations are inhibiting aspects of particle

assembly, budding, or release. Additionally, these mutants showed a complete loss of infectivity with normalize levels of particles were presented to MAGI cells **(Fig. 4).** Gag subcellular distribution showed a more nuclear and perinuclear localization of Gag for the G38M and N127E mutants as compared to WT Gag **(Fig. 5).** Direct visualization of the produced immature particles showed an absence of electron density below the lipid bilayer of immature particles **(Fig. 6).** In another analysis looking directly at the ability of CA to form oligomers it was observed that these two mutants significantly disrupt HIV-2 CA-NC protein assembly *in vitro* with no ordered assemblies present **(Fig. 7)**. To probe the structural basis of these results we looked at molecular interfaces in HIV-1 lattice structures from immature and mature particles. For HIV-1 it appeared that N128 was in close proximity to E44 at the Using this structural comparison we chose to mutate E44, the equivalent HIV-2 residue that app with the N127 based on HIV CA structure, and found that two single mutations result in significant particle reduction, but the double mutation had a partial rescue that suggests these residues may be involved in a direct interaction in the immature Gag lattice. This indicated an undiscovered interaction in HIV-2 between E44 and N127 that has not previously observed in HIV-1, which played an essential role in Gag-Gag interactions.

Our results indicated that relatively minor changes such as one residue change could profoundly impact overall particles. Non-conserved residues such as G38 and N127 might play an important role in HIV-2 CA structure and Gag-Gag interactions. Intriguingly, G38 and N127 are critical residues in the HIV-2 CA 3-fold inter-hexamer interface, and this suggested that the 3-fold interface is likely to play a critical role in Gag-Gag interactions.

However, a potential limitation of our analysis is that not all residues in HIV-2 CA were mutated and examined. We tried to choose residues with different critical parameters, (i) at a different location: inter-domain linker, intra-hexamer interface, and inter-hexamer interface (2-fold interface & 3-fold interface); (ii) conserved and non-conserved residues; (iii) residues at helix and loop; (iv) previously reported and not reported. Furthermore, future studies such as analyzing multi-cycle infectivity, reversion mutations in replication-competent virus, and screening for second site revertants will likely provide other surprising observations that enhance our understanding of the molecular interactions involved in virus assembly.

Taken together, the observations complemented structural analyses of HIV-2 particles and Gag lattice organization, providing insights into the morphological differences between HIV-1 and HIV-2 immature particles and their impact on virus replication. Our studies emphasized the differences between HIV-1 and HIV-2 regarding particle assembly and the importance of CA interactions for retroviral assembly.

MATERIALS AND METHODS

Plasmids, cell lines, and reagents

HIV-2 Gag genes in the *pN3-Gag* and *pEYFP-N3-Gag* vectors and HIV-2 Env expression plasmid have been previously described [38]. HeLa and HEK293T/17 cells lines were purchased from ATCC (Manassas, VA) and cultured in Dulbecco's modified Eagle medium (DMEM) supplemented with 10% fetal clone III (FC3; GE Healthcare Lifesciences, UT) and 1% Penicillin-Streptomycin (Pen Strep; Invitrogen, CA) at 37 °C in 5% CO_2. *pNL4-3 MIG* [47] and *pROD-MIG* [48] have been previously described. Viruses were pseudotyped with the VSV-G expression construct, *pHCMV-G* (San Diego, CA). U373-MAGI-CXCR4$_{CEM}$ cells (NIH AIDS Reagent Program, NIAID, NIH) were maintained similarly to HEK293T/17 cells but with 1.0 µg/mL puromycin, 0.1 mg/mL hygromycin B, and 0.2 mg/mL neomycin to the medium. All cells used in this study were certified mycoplasma free.

Site-directed mutagenesis of gag plasmids

A panel of 21 alanine-scanning HIV-2 CA mutants was engineered by mutating the HIV-2 *pN3-Gag* plasmid (except A42D) to alanine-encoding codons using the Gibson assembly method as previously described [49]. A panel of 10 non-conserved HIV-2 mutants was generated by changing the codons in HIV-2 to HIV-1 NL4-3 residues, based on HIV-2 *pN3-Gag* vectors. The mutants of interest were also engineered into the pEYFP-N3-Gag, pROD-MIG, and pET28a plasmid backbones for cellular localization, infectivity, and in vitro assembly assays respectively. All mutants were confirmed by Sanger sequencing. See **Fig. 1A** for mutation sites.

Immature particle production

The efficiency of immature particle production was analyzed by quantifying the Gag proteins in culture supernatants using immunoblot with mouse monoclonal anti-HIV-1 p24 antibody (Catalogue #: sc-69728; Santa Cruz Biotechnology, TX). Briefly, the *pN3-HIV-2-Gag* plasmid and the HIV-2 Env expression plasmid were co-transfected into HEK293T/17 cells using GenJet, ver II (SignaGen, Gaithersburg, MD) at a 10:1 ratio, respectively. After 48-hours post-transfection, the viral supernatants were harvested, clarified by centrifugation (1,800 × g for 10 min), and filtered through 0.2 µm filters. Then the supernatants were concentrated by ultracentrifugation in a 50.2 Ti rotor (Beckman Coulter, CA) at 211,400 × g for 90 min through an 8% Opti-prep (Sigma-Aldrich, MO) cushion. The VLPs were resuspended in 1× STE buffer (100 mM NaCl, 10 mM Tris pH 8.0, and 1 mM EDTA) (G-Biosciences, MO). The 293T/17 cells were collected and lysed with the RIPA lysis buffer and clarified via centrifugation (1800 x g for 10 min). The protein concentrations were measured using the BCA assay (Peirce, WI) before the samples were subjected to SDS-PAGE and transferred to nitrocellulose membranes. Gag

proteins were detected with a 1:5,000 dilution of anti-HIV p24 antibody in 2.5% milk TBST (tris buffer saline plus tween-20). Glyceraldehyde 3-phosphate dehydrogenase (GAPDH) was detected with 1:1,000 anti-GAPDH hFAB™ Rhodamine antibody (Bio-rad, CA) in 2.5% milk TBST (tris buffer saline plus tween-20). Membranes were washed before incubation with goat anti-mouse StarBright™ Blue 700 secondary. Gag levels from cells will be normalized relative to GAPDH levels, and the mutant Gag expression levels were determined relative to WT.

The efficiency of mature particle production was analyzed by quantifying the CA (p24) band in culture supernatants using the same antibodies as the immature particle production analysis. Briefly, the HIV-2 *pROD-MIG* plasmids and the VSV-G expression construct were co-transfected into HEK293T/17 cells using GenJet ver II at a 3:1 ratio to produce WT and mutant infectious viral particles. After 48-hours post-transfection, the viral supernatants were harvested, clarified by centrifugation (1,800 × g for 10 min), and filtered through 0.2 µm filters. Then the supernatants were concentrated by ultracentrifugation in a 50.2 Ti rotor (Beckman Coulter, CA) at 211,400 × g for 90 min through an 8% Opti-prep (Sigma-Aldrich, MO) cushion. Capsid proteins were detected with a 1:1,500 anti-HIV p24 antibody. Glyceraldehyde 3-phosphate dehydrogenase (GAPDH) was detected with 1:1,000 anti-GAPDH hFAB™ Rhodamine antibody (Bio-rad, CA). CA levels from cells will be normalized relative to GAPDH levels, and the mutant CA expression levels were determined relative to WT. Membranes were washed before incubation with 1:3, 000 goat anti-mouse StarBright™ Blue 700 (Bio-Rad, CA).

For all blot analysis, membranes were imaged with a ChemiDoc Touch system (Bio-Rad, CA) and analyzed with ImageJ. Quantified results were presented using GraphPad Prism 6.0 (GraphPad Software, Inc., CA). Significance relative to WT was determined by an unpaired t-test. Immunoblots were performed with three independent replicates.

Gag subcellular distribution analysis

Gag subcellular distribution was analyzed by quantifying the degree of Gag protein assembly into puncta using confocal laser scanning microscopy techniques. Subcellular localization of Gag-eYFP was evaluated as previously described [50]. Briefly, HeLa cells were cultured in six-well plates on no. 1.5 standard glass coverslips coated with poly-l-lysine, and experiments were performed as previously described [50]. HeLa cells were transiently transfected with eYFP-tagged Gag and untagged Gag expression plasmids at a 1:4 ratio using GenJet, ver II (SignaGen, Gaithersburg, MD). After 48-hours post-transfection, cells were stained with DAPI (Thermo Fisher Scientific, MA) and ActinRed 555 (Invitrogen, CA) before fixation with 4% paraformaldehyde (Thermo Fisher Scientific, MA). Cells were imaged via a Zeiss LSM 700 confocal laser scanning microscope using a Plan-Apochromat 63×/1.40-

numeric-aperture (NA) oil objective at 1.2× zoom (Carl Zeiss, Oberkochen, Germany). At least 5 individual cells were imaged across three independent replicates for a total of 15 cells, and WT Gag-eYFP served as a positive control for WT levels of Gag puncta formation.

Cryo-EM analysis of particle morphology.

The *pN3-HIV-2-Gag* plasmid and the HIV-2 Env expression plasmids were co-transfected into HEK293T/17 cells using GenJet, ver II (SignaGen, Gaithersburg, MD) at a 10:1 ratio as previously described [38]. After 48-hours post-transfection, the viral supernatants were harvested and centrifuged at 1,800 × g for 5 min and followed by passing through a 0.2 µm filter. VLPs were then concentrated from the supernatants by ultracentrifugation in a 50.2 Ti rotor (Beckman Coulter, CA) at 211,400 × g for 90 min through an 8% Opti-prep (Sigma-Aldrich, MO) cushion. The VLP pellets were resuspended in ~200 µl STE buffer before centrifuging over a 10% to 30% Opti-Prep step gradient at 301,090 x g for 3 hours. The visible viral particle band was extracted from the gradient and pelleted in STE buffer at 267,636 × g for 1 h using an SW55 Ti rotor. The pellet was then resuspended in ~10 µl STE buffer and frozen at -80°C. These samples were analyzed by cryo-EM. The experiments were independently repeated three times. The particle samples were firstly screened by negative staining TEM with 0.75 % (w/v) uranyl formate for determining viral particle concentration on a 120 kV Tecnai Spirit TEM [51].

HIV-2 Gag WT and mutant VLP samples were prepared for cryo-EM as previously described [38, 50, 52]. Briefly, the VLP samples were thawed on ice, and approximately 3.5 µL of purified HIV-2 Gag VLPs were applied to freshly glow-discharged (10 mA for 30 sec using a Leica Ace600 glow-discharger) Quantifoil R2/1 300-mesh holey carbon-coated copper grids. The grids were then blotted for 4-10 sec with filter paper at 19°C with 85% relative humidity and plunge-frozen in liquid ethane using a FEI Mark III Vitrobot or Leica GP-2 grid plunger. The frozen grids were stored in liquid nitrogen until imaging analysis.

The frozen grids were imaged for cryo-EM analysis on a Tecnai FEI G2 F30 FEG transmission electron microscope (FEI, OR) at liquid nitrogen temperature operating at 300 kV. Images were recorded at a nominal magnification of 39,000x and 59,000x magnification under ~25 electrons/Å^2 conditions at 1 to 5 µm under-focus using a Gatan Slow Scan 4k by 4k charge-coupled-device (CCD) camera or a Gatan K2 Summit direct electron detector (Gatan Inc., Pleasanton, CA).

Infectivity assay

The HIV-2 *pROD-MIG* plasmids and the VSV-G expression construct were co-transfected into HEK293T/17 cells using GenJet, ver II (SignaGen, Gaithersburg, MD) at a 3:1 ratio to produce WT and mutant infectious viral particles. After 48-hours post-transfection, the viral

supernatants were harvested, clarified by centrifugation (1,800 × g for 10 min), and filtered through 0.2 µm filters. U373-MAGI-CXCR4 cells were plated in a 12-well plate and each well treated with 1 ml viral supernatants and 1 ml fresh medium. Each group had 4 well replicates. The cells were collected for fluorescence analysis via BD LSR II flow cytometer (BD Biosciences) 48-hours post-infection as described before [42]. Flow cytometry data were examined in FlowJo v.7 (Ashland, OR). The infectious cells were calculated from the flow data by adding all positive quadrants (mCherry+ only, GFP+ only, and mCherry+/GFP+) to determine infectivity. Mutant infection level was determined related to WT. Then, the relative infectivity of each group was normalized to its relative mature particle production as assessed by p24 immunoblot of the produced particles. Three independent experiments were performed.

In vitro HIV-2 CA-NC assembly analysis

HIV-2 CA-NC (Gag amino acids 136-431) was cloned into a pET28a backbone vector, and capsid mutants were engineered using Gibson assembly reactions. The proteins were purified following a previously described protocol for purifying nucleocapsid domain-containing HIV-1 Gag proteins [44, 45]. Briefly, the CA-NC protein was expressed in BL21 (DE3) RIP pLysS *E. coli* cells grown in 1L of ZY-auto induction media for 16 hours shaking at 37C [53]. Cells were resuspended in 50 mL lysis buffer per 1 L culture (500 mM NaCl, 25 mM Tris pH 7.5, 1 µM $ZnCl_2$, 10 mM β-Mercaptoethanol (BME)) and flash frozen. After thawing, cells were lysed by adding 10 mg lysozyme, 0.1% triton (v/v), and sonicated with 10 sec on/off cycles at 40% amplitude for three 10 min treatments to reduce viscosity. The supernatant was clarified with a 12,000 × g 40 min spin. Nucleic acids were removed using polyethyleneimine (PEI), and the protein was precipitated with saturated ammonium sulfate using 1/3 (v/v) of the total supernatant volume. The precipitated protein was pelleted using a 10,000 × g spin for 15 min. The precipitate was resuspended in 50 mM NaCl, 25 mM Tris, 5 µM $ZnCl_2$, 10 mM BME, pH 7.5, and further dialyzed against 1L for 1 hour at 4C. The protein was concentrated using Amicon ultra-15 centrifugal filter unit concentrator (Millipore) and loaded onto an ion-exchange column (HiTrap SP FF, Cytiva, Global Life Sciences Solutions USA LLC, MA). The protein was eluted using a linear NaCl gradient from 50-700 mM. Fractions containing the protein were pooled, concentrated to ~10 mg/mL, and flash frozen in liquid nitrogen.

For the assembly assay, the purified protein was diluted to 50 µM in 250 mM NaCl, 50 mM Tris, pH 8. A 50-mer oligonucleotide consisting of 25 (GT) repeats were added at a final concentration of 5 µM. The protein was dialyzed against assembly buffer (2M NaCl, 50 mM Tris, 150 µM IP6, 5 µM $ZnCl_2$, pH 8) at room temperature in Pierce™ Slide A Lyzer® Mini Dialysis Units. Turbidity measurements at A340 nm were used to quantify the reaction progress via

NanoDrop 1000 Spectrophotometer (Thermo Fisher Scientific, MA). Readings were taken every 20 minutes for 2 hours and corrected for any changes in reaction volume due to dialysis.

After 2-hour dialysis, 3 µl of each reaction were spotted on EMS CF300-CU grids (Ted Pella, CA) for 2 minutes. The sample was blotted with filter paper, washed 3x in deionized water, blotted, and stained in 0.75% (w/v) uranyl formate for 2 minutes. Samples were imaged on an FEI Technai Spirit Bio-Twin transmission electron microscope at 120 kV.

1. Del Rio, C., *The global HIV epidemic: What the pathologist needs to know.* Semin Diagn Pathol, 2017. **34**(4): p. 314-317.
2. Campbell-Yesufu, O.T. and R.T. Gandhi, *Update on human immunodeficiency virus (HIV)-2 infection.* Clin Infect Dis, 2011. **52**(6): p. 780-7.
3. Nyamweya, S., et al., *Comparing HIV-1 and HIV-2 infection: Lessons for viral immunopathogenesis.* Rev Med Virol, 2013. **23**(4): p. 221-40.
4. Andersson, S., et al., *Plasma Viral Load in HIV-1 and HIV-2 Singly and Dually Infected Individuals in Guinea-Bissau, West Africa.* Arch Intern Med, 2000. **160**(21): p. 3286-3293.
5. de Silva, T.I., M. Cotten, and S.L. Rowland-Jones, *HIV-2: the forgotten AIDS virus.* Trends Microbiol, 2008. **16**(12): p. 588-95.
6. van der Loeff, M.F., et al., *Undetectable plasma viral load predicts normal survival in HIV-2-infected people in a West African village.* Retrovirology, 2010. **7**: p. 46.
7. Spearman, P., *HIV-1 Gag as an Antiviral Target: Development of Assembly and Maturation Inhibitors.* Curr Top Med Chem, 2016. **16**(10): p. 1154-1166.
8. Freed, E.O., *HIV-1 assembly, release and maturation.* Nat Rev Microbiol, 2015. **13**(8): p. 484-96.
9. Briant, L., et al., *HIV-1 Assembly, Release and Maturation.* World Journal of AIDS, 2011. **01**(04): p. 111-130.
10. Sundquist, W.I. and H.G. Krausslich, *HIV-1 assembly, budding, and maturation.* Cold Spring Harb Perspect Med, 2012. **2**(7): p. a006924.
11. Gheysen, D., et al., *Assembly and Release of HIV-1 Precursor Pr5Wg Virus-like Particles from Recombinant Baculovirus-Infected Insect Cells.* Cell, 1989. **59**: p. 103-112.
12. Chen, B., *HIV Capsid Assembly, Mechanism, and Structure.* Biochemistry, 2016. **55**(18): p. 2539-52.
13. Molina, J.M., et al., *Efficacy and safety of long-acting subcutaneous lenacapavir in phase 2/3 in heavily treatment-experienced people with HIV: week 26 results (Capella study).* Journal of the International AIDS Society, 2021. **24**: p. 75+.
14. Gottlieb, G.S., et al., *Emergence of multiclass drug-resistance in HIV-2 in antiretroviral-treated individuals in Senegal: implications for HIV-2 treatment in resouce-limited West Africa.* Clin Infect Dis, 2009. **48**(4): p. 476-83.
15. Smith, R.A., et al., *Antiretroviral drug resistance in HIV-2: three amino acid changes are sufficient for classwide nucleoside analogue resistance.* J Infect Dis, 2009. **199**(9): p. 1323-6.
16. Maldonado, J.O., et al., *New insights into retroviral Gag-Gag and Gag-membrane interactions.* Front Microbiol, 2014. **5**: p. 302.
17. Chukkapalli, V., et al., *Interaction between the human immunodeficiency virus type 1 Gag matrix domain and phosphatidylinositol-(4,5)-bisphosphate is essential for efficient gag membrane binding.* J Virol, 2008. **82**(5): p. 2405-17.
18. Kafaie, J., et al., *Mapping of nucleocapsid residues important for HIV-1 genomic RNA dimerization and packaging.* Virology, 2008. **375**(2): p. 592-610.
19. Grime, J.M.A., et al., *Coarse-grained simulation reveals key features of HIV-1 capsid self-assembly.* Nat Commun, 2016. **7**: p. 11568.
20. Briggs, J.A. and H.G. Krausslich, *The molecular architecture of HIV.* J Mol Biol, 2011. **410**(4): p. 491-500.
21. Schur, F.K., et al., *Structure of the immature HIV-1 capsid in intact virus particles at 8.8 A resolution.* Nature, 2015. **517**(7535): p. 505-8.
22. Zhao, G., et al., *Mature HIV-1 capsid structure by cryo-electron microscopy and all-atom molecular dynamics.* Nature, 2013. **497**(7451): p. 643-6.
23. Gres, A.T., et al., *X-ray crystal structures of native HIV-1 capsid protein reveal conformational variability.* Science, 2015. **349**(6243): p. 99-103.

24. Pornillos, O., et al., *X-ray structures of the hexameric building block of the HIV capsid.* Cell, 2009. **137**(7): p. 1282-92.
25. Pornillos, O., B.K. Ganser-Pornillos, and M. Yeager, *Atomic-level modelling of the HIV capsid.* Nature, 2011. **469**(7330): p. 424-7.
26. Briggs, J.A., et al., *Cryo-electron microscopy reveals conserved and divergent features of gag packing in immature particles of Rous sarcoma virus and human immunodeficiency virus.* J Mol Biol, 2006. **355**(1): p. 157-68.
27. Qu, K., et al., *Structure and architecture of immature and mature murine leukemia virus capsids.* Proc Natl Acad Sci U S A, 2018. **115**(50): p. E11751-E11760.
28. Briggs, J.A., et al., *Structure and assembly of immature HIV.* Proc Natl Acad Sci U S A, 2009. **106**(27): p. 11090–11095.
29. von Schwedler, U.K., et al., *Functional surfaces of the human immunodeficiency virus type 1 capsid protein.* J Virol, 2003. **77**(9): p. 5439-50.
30. Meng, X., et al., *Protease cleavage leads to formation of mature trimer interface in HIV-1 capsid.* PLoS Pathog, 2012. **8**(8): p. e1002886.
31. Srinivasakumar, N., M.L. Hammarskjöld, and D. Rekosh, *Characterization of deletion mutations in the capsid region of human immunodeficiency virus type 1 that affect particle formation and Gag-Pol precursor incorporation.* J Virol, 1995. **69**(10): p. 6106-6114.
32. Doi, N., et al., *Role for Gag-CA Interdomain Linker in Primate Lentiviral Replication.* Front Microbiol, 2019. **10**: p. 1831.
33. Strambio-de-Castillia, C. and E. Hunter, *Mutational analysis of the major homology region of Mason-Pfizer Monkey Virus by use of saturation mutagenesis.* J Virol, 1992. **66**(12): p. 7021-7032.
34. Craven, R.C., et al., *Genetic analysis of the major homology region of the Rous Sarcoma Virus Gag protein.* J Virol, 1995. **69**(7): p. 4213-4227.
35. Ganser-Pornillos, B.K., et al., *Assembly properties of the human immunodeficiency virus type 1 CA protein.* J Virol, 2004. **78**(5): p. 2545-52.
36. Shoko Nakanishi, S.W., Naoya Doi, Takaaki Koma, Akio Adachi, Masako Nomaguchi, *Virological characterization of HIV-1 CA-NTD mutants constructed in a virus-lineage reflected manner.* The Journal of Medical Investigation, 2018. **65**(1.2): p. 110-115.
37. Zhang, W., et al., *Morphology and ultrastructure of retrovirus particles.* AIMS Biophys, 2015. **2**(3): p. 343-369.
38. Martin, J.L., et al., *Distinct Particle Morphologies Revealed through Comparative Parallel Analyses of Retrovirus-Like Particles.* J Virol, 2016. **90**(18): p. 8074-84.
39. Miyazaki, Y., et al., *Comparison of Biochemical Properties of HIV-1 and HIV-2 Capsid Proteins.* Front Microbiol, 2017. **8**: p. 1082.
40. Tanaka, M., et al., *Mutations of Conserved Residues in the Major Homology Region Arrest Assembling HIV-1 Gag as a Membrane-Targeted Intermediate Containing Genomic RNA and Cellular Proteins.* J Virol, 2016. **90**(4): p. 1944-63.
41. Donna L. Mallery, A.B.K., Nadine Renner, K. M. Rifat Faysal, Mariia Novikova, Leo Kiss, Miranda S. C. Wilson, Bilal Ahsan, Zunlong Ke, John A. G. Briggs, Adolfo Saiardi, Till Böcking, Eric O. Freed, and Leo C. James, *A stable immature lattice packages IP6 for HIV capsid maturation.* Sci Adv, 2021. **7**(11): p. eabe4716.
42. Rawson, J.M., C.L. Clouser, and L.M. Mansky, *Rapid Determination of HIV-1 Mutant Frequencies and Mutation Spectra Using an mCherry/EGFP Dual-Reporter Viral Vector.* Methods Mol Biol, 2016. **1354**: p. 71-88.
43. Dostalkova, A., et al., *A simple, high-throughput stabilization assay to test HIV-1 uncoating inhibitors.* Sci Rep, 2019. **9**(1): p. 17076.

44. Kucharska, I., et al., *Biochemical Reconstitution of HIV-1 Assembly and Maturation.* J Virol, 2020. **94**(5).
45. Barbie K. Ganser, S.L., Victor Y. Klishko, John T. Finch, Wesley I. Sundquist, *Assembly and Analysis of Conical Models for the HIV-1 Core.* Science, 1999. **283**(5398): p. 80-83.
46. Jiang, J., et al., *The interdomain linker region of HIV-1 capsid protein is a critical determinant of proper core assembly and stability.* Virology, 2011. **421**(2): p. 253-65.
47. Clouser, C.L., S.E. Patterson, and L.M. Mansky, *Exploiting drug repositioning for discovery of a novel HIV combination therapy.* J Virol, 2010. **84**(18): p. 9301-9.
48. Beach, L.B., et al., *Novel inhibitors of human immunodeficiency virus type 2 infectivity.* J Gen Virol, 2014. **95**(Pt 12): p. 2778-83.
49. Heydenreich, F.M., et al., *High-throughput mutagenesis using a two-fragment PCR approach.* Sci Rep, 2017. **7**(1): p. 6787.
50. Martin, J.L., et al., *Critical Role of the Human T-Cell Leukemia Virus Type 1 Capsid N-Terminal Domain for Gag-Gag Interactions and Virus Particle Assembly.* J Virol, 2018. **92**(14).
51. Thompson, R.F., et al., *An introduction to sample preparation and imaging by cryo-electron microscopy for structural biology.* Methods, 2016. **100**: p. 3-15.
52. Martin, J.L., et al., *Disparate Contributions of Human Retrovirus Capsid Subdomains to Gag-Gag Oligomerization, Virus Morphology, and Particle Biogenesis.* J Virol, 2017. **91**(14).
53. Studier, F.W., *Protein production by auto-induction in high density shaking cultures.* Protein Expr Purif, 2005. **41**(1): p. 207-34.
54. Madeira, F., et al., *The EMBL-EBI search and sequence analysis tools APIs in 2019.* Nucleic Acids Res, 2019. **47**(W1): p. W636-W641.
55. Price, A.J., et al., *Active site remodeling switches HIV specificity of antiretroviral TRIMCyp.* Nat Struct Mol Biol, 2009. **16**(10): p. 1036-42.
56. Buchan, D.W.A. and D.T. Jones, *The PSIPRED Protein Analysis Workbench: 20 years on.* Nucleic Acids Res, 2019. **47**(W1): p. W402-W407.
57. Jones, D.T., *Protein secondary structure prediction based on position-specific scoring matrices.* J Mol Biol, 1999. **292**(2): p. 195-202.

682 **Figure 1**

683

684 **A**

```
                                Helix 1          Helix 2      Helix 3
HIV-1   1   PIVQNLQGQMVHQAISPRTLNAWVKVVEEKAFSPEVIPMFSALSEGATPQDLNTMLNTVGGH  62
            * **:: *: .*  :**********:**** *. **:* *.*****.** *:* *** **.*
HIV-2   1   P-VQHVGGNYTHIPLSPRTLNAWVKLVEEKKFGAEVVPGFQALSEGCTPYDINQMLNCVGDH  61

                      Helix 4                        Helix 5      Helix 6
HIV-1   63  QAAMQMLKETINEEAAEWDRLHPVHAGPIAPGQMREPRGSDIAGTTSTLQEQIGWMTH-N  121
            *****:::* *********  **:  **:  **:***************::*** ** : :
HIV-2   62  QAAMQIIREIINEEAAEWDVQHPI-PGPLPAGQLREPRGSDIAGTTSTVEEQIQWMFRPQ  120

                        Helix 7                                Helix 8   Helix 9
HIV-1   122 PPIPVGEIYKRWIILGLNKIVRMYSPTSILDIRQGPKEPFRDYVDRFYKTLRAEQASQEV  181
             *:***:**:*** :**:* ****.**.****:*******:.*******:*****:.  *
HIV-2   121 NPVPVGNIYRRWIQIGLQKCVRMYNPTNILDIKQGPKEPFQSYVDRFYKSLRAEQTDPAV  180

                   Helix 9    Helix 10        Helix 11    Helix 12
HIV-1   182 KNWMTETLLVQNANPDCKTILKALGPGATLEEMMTACQGVGGPGHKARVL  231
            *****:************ :**.** . *****:**********:***::
HIV-2   181 KNWMTQTLLVQNANPDCKLVLKGLGMNPTLEEMLTACQGVGGPGQKARLM  230
```

685

686 **B** **C**

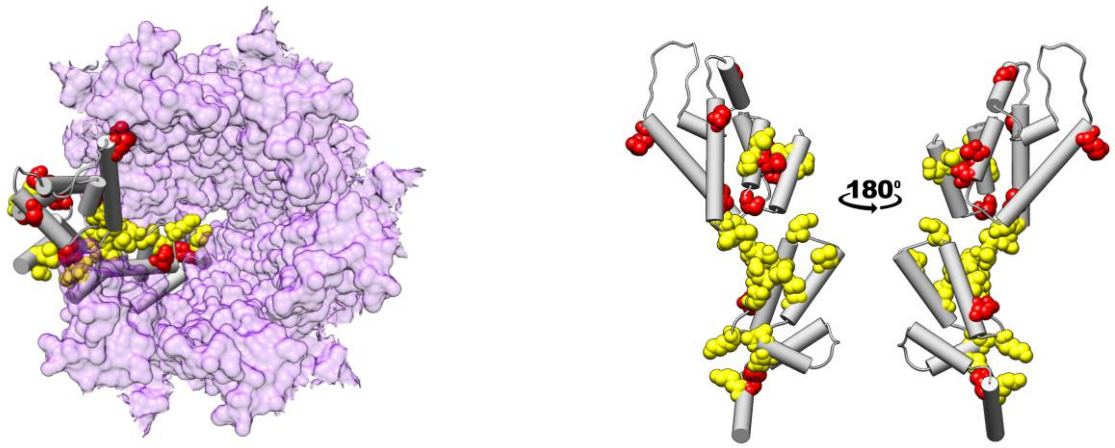

687

688

689 **Figure 1. (A) Alignment of HIV-1 and HIV-2 CA sequences.** Amino acid sequences in CA of
690 HIV-1 NL4-3 (GenBank accession no. AF324493; CA 1-231; Gag 133-363) and HIV-2 ROD
691 (GenBank accession no. M15390; CA 1- 230; Gag 136-365) were aligned by Clustal Omega
692 Multiple Sequence Alignment [54]. Locations of HIV-1 immature CA helices in this alignment are
693 as described previously [21] (PDB ID: 5L93) and indicated by black boxes. HIV-2 immature
694 CA_{NTD} (CA 1-144; Gag 136-279) helices are as described previously [55] (PDB ID: 2WLV), and
695 indicated with blue boxes. CA_{CTD} (CA 145-230; Gag 280-365) helices are predicted by the
696 PSIPRED server [56, 57], indicated by green boxes. "*" indicates conserved amino acids; ":"
697 indicates amino acid substitution with high amino acid similarity; "." indicates amino acid
698 substitutions with low similarity. Yellow highlight indicates alanine-scanning mutagenesis on
699 conserved residues. Red highlight indicates mutagenesis on non-conserved residues, which
700 HIV-2 residues were mutated to HIV-1 types. **(B) Structure of CA hexamer.** Mutagenesis of
701 conserved residues were colored yellow, and mutagenesis of non-conserved residues were
702 colored red. **(C) Structure of CA monomer.**
703
704

Figure 2

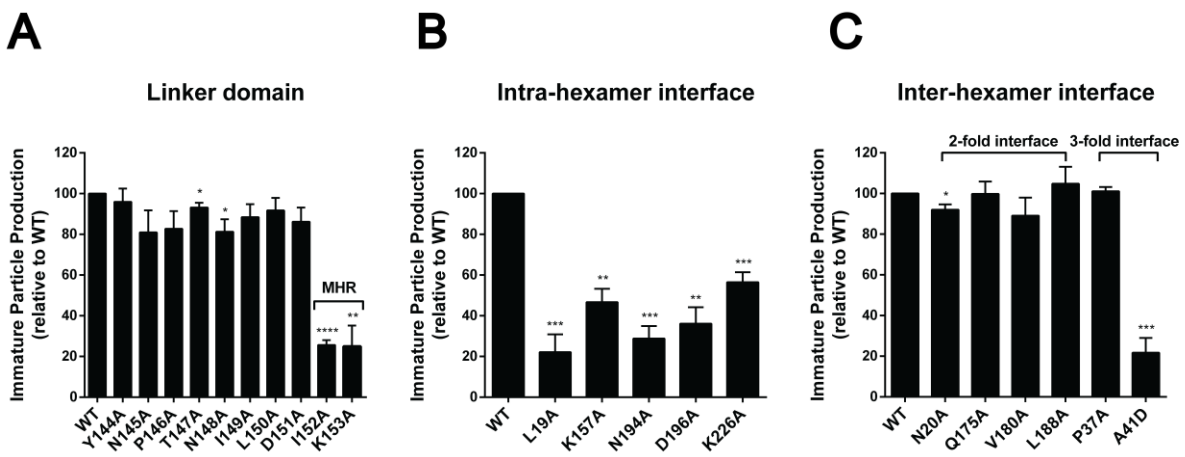

Figure 2. Relative immature particle production of HIV-2 CA mutants at CA_{NTD}-CA_{CTD} linker (A), intra-hexamer interface (B), and inter-hexamer interface (C). 293T/17 cells were transfected with untagged HIV-2 Gag expression constructs (WT or alanine-scanning mutants), and the cell culture supernatants were harvested 48h post transfection. Immunoblot analysis was conducted to determine the amount of immature particle production for WT and CA conserved mutants. The relative particle production of CA mutants was calculated relative to WT. Histograms are presented to indicate the relative immature particle production of HIV-2 CA alanine-scanning mutants. Error bars represent standard error of the mean from three independent experiments. Significance relative to WT was determined by unpaired t test. ****, $P < 0.0001$; ***, $P < 0.001$; **, $P < 0.01$; *, $P < 0.05$. MHR = Major homology region.

Figure 3

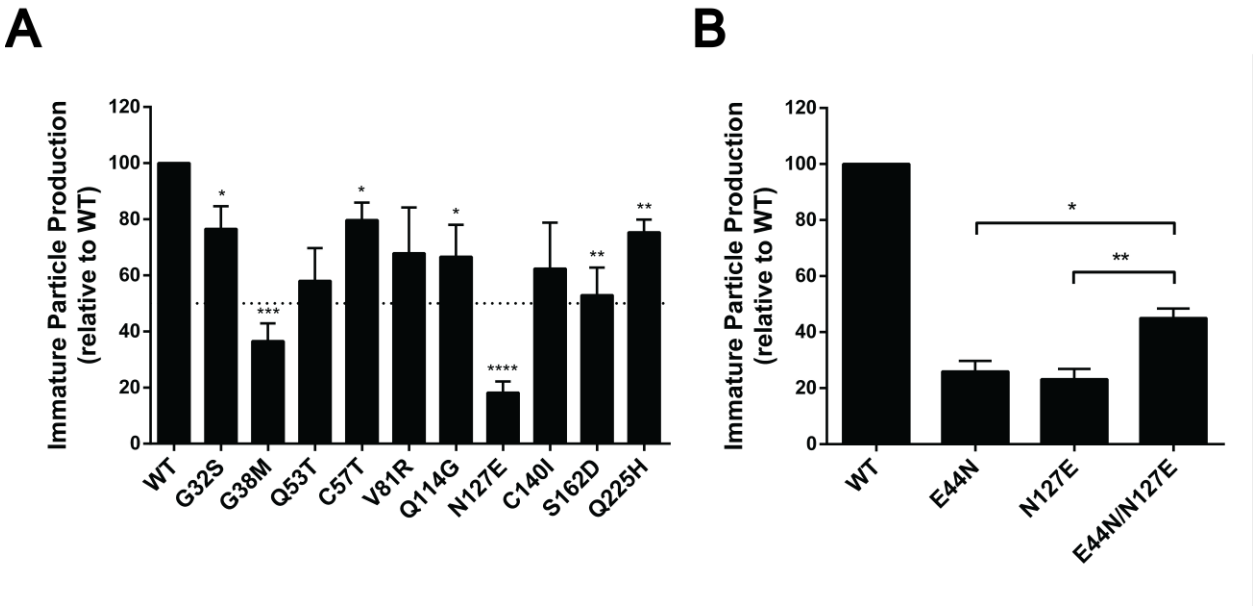

Figure 3. Relative immature particle production for a panel of HIV-2 CA mutants on non-conserved residues. (A) Relative immature production of HIV-2 non-conserved residue mutants. (B) Relative immature particle production of HIV-2 CA E44N, N127E and E44N/N127E. 293T/17 cells were transfected with untagged HIV-2 Gag expression constructs (WT or mutants), and the cell culture supernatants were harvested 48h post transfection. Immunoblot analysis was conducted to determine the amount of particle production for WT and mutants. The relative immature particle production of CA mutants were calculated relative to WT. Histograms are presented to indicate the relative particle production of HIV-2 CA mutants. Error bars represent standard error of the mean from three independent experiments. Significance relative to WT was determined by unpaired t test. ****, $P < 0.0001$; ***, $P < 0.001$; **, $P < 0.01$; *, $P < 0.05$.

738 **Figure 4**

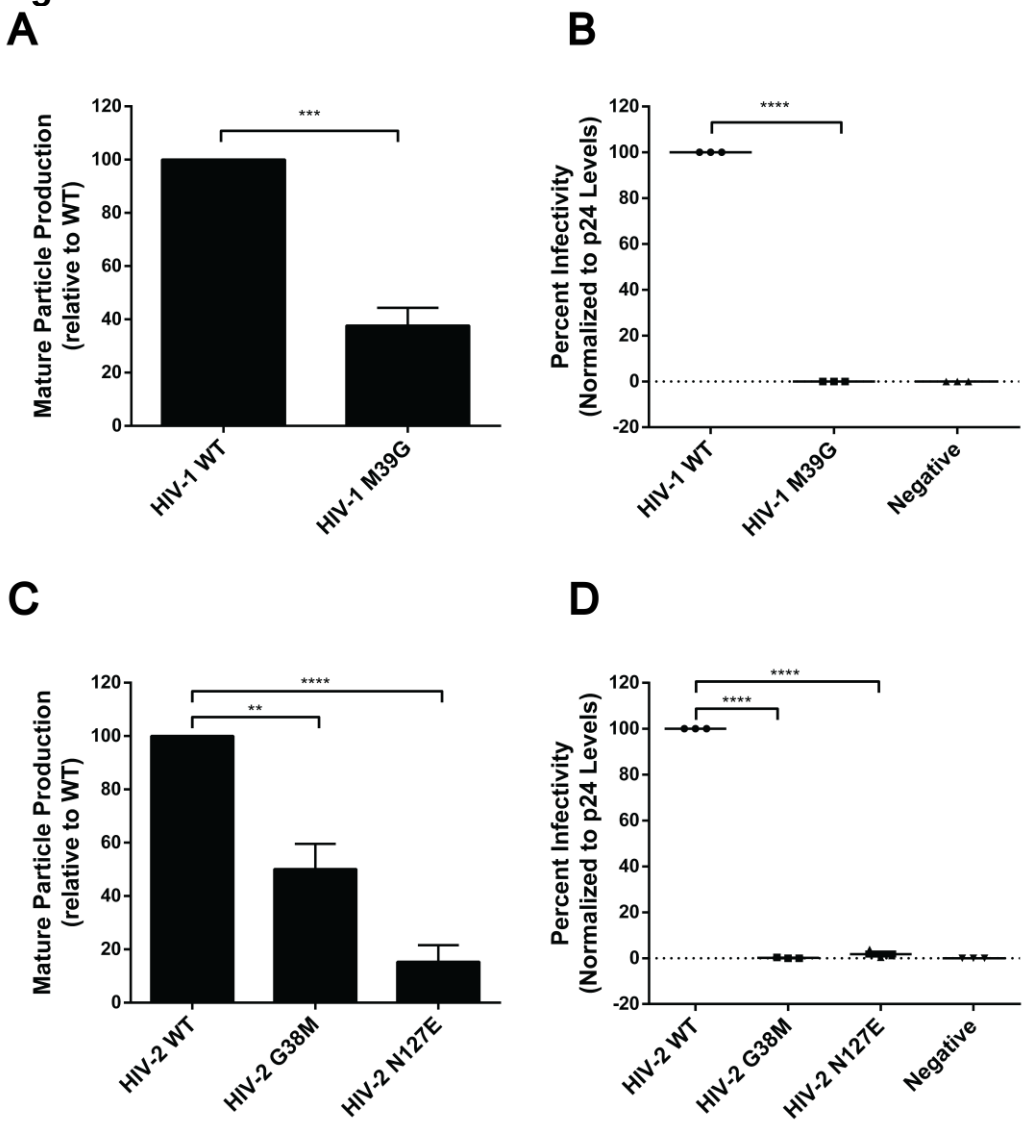

739
740 **Figure 4. Relative mature particle production and infectivity analysis.** 293T/17 cells were
741 transfected with HIV-1 NL43 MIG (A,B) or HIV-2 ROD MIG (C,D) constructs (WT or mutants)
742 and VSVG, and the mature particles were harvested from the cell culture supernatants. (A,C)
743 Relative mature particle production. Immunoblot analysis was conducted to determine the
744 amount of particle production for WT and mutants. HIV CA was evaluated by detection with an
745 StarBright™ Blue 700 secondary antibody. (B,D) Relative infectivity. MAGI cells were then
746 challenged with HIV MIG-VSVG viral supernatants or fresh medium (Negative control) and
747 collected 48 h postinfection. Infectivity was determined by flow cytometry analysis for
748 expression of GFP and mCherry, which are both encoded by the vectors. Relative infectivity
749 was determined and normalized to particle production. Error bars represent standard deviations
750 from three independent experiments. Significance relative to WT was determined by unpaired t
751 test. ****, $P < 0.0001$; ***, $P < 0.001$; **, $P < 0.01$.
752

Figure 5

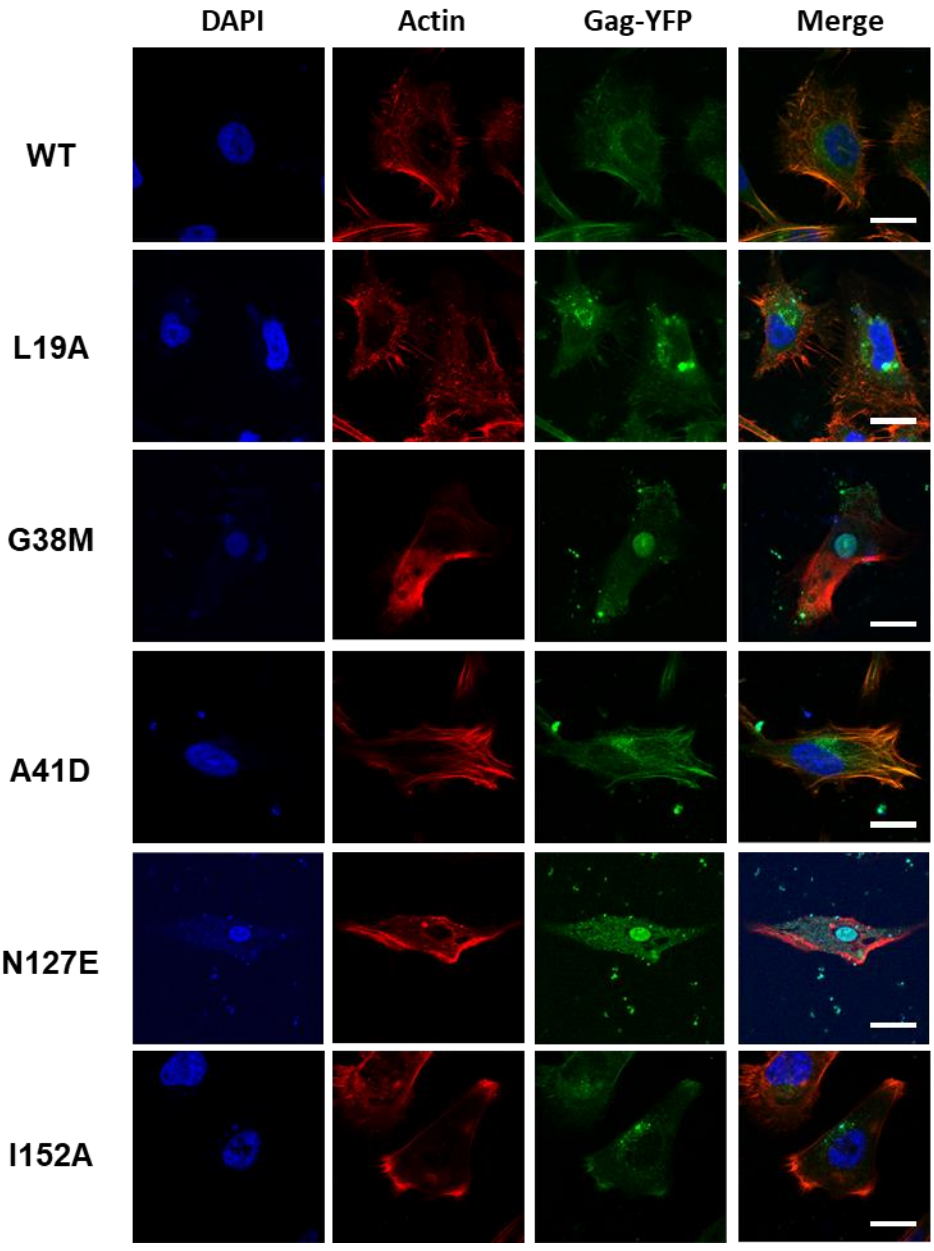

Figure 5. Subcellular distribution of HIV-2 Gag for CA mutants. HeLa cells were transfected with a WT HIV-2 Gag-eYFP or the indicated mutant Gag. Representative images for WT HIV-2 Gag-eYFP and for the mutants L19A, G38M, A41D, N127E and I152A are shown. At least 15 individual cells were imaged across three independent replicates for a total of 15 cells. Scale bar, 20 μm.

Figure 6

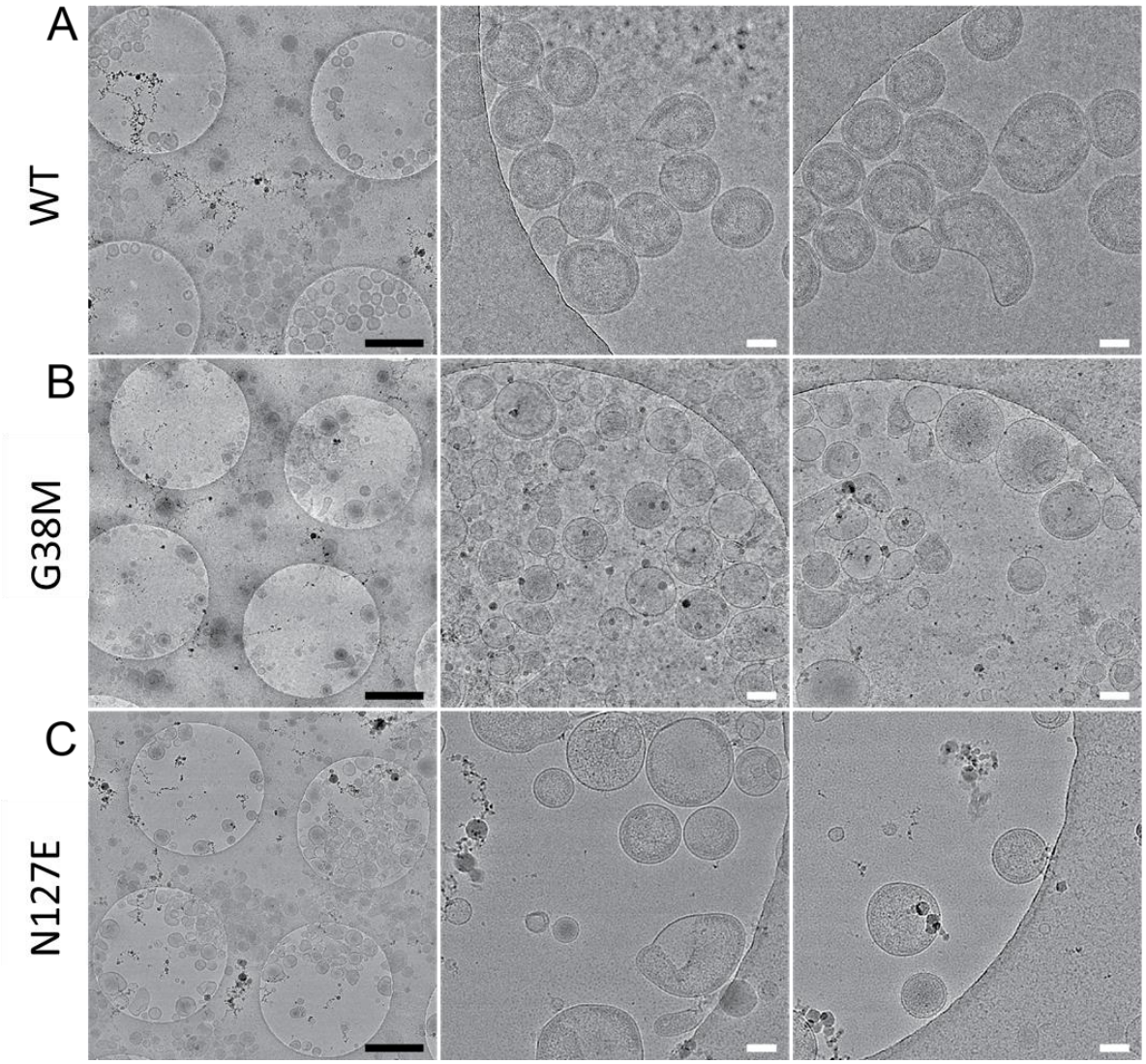

Figure 6. Cryo-EM images of VLPs produced by selected CA mutants. 293T/17 cells were transfected with untagged HIV-2 Gag expression constructs (WT or selected mutants), and the immature particles were concentrated and purified from cell culture supernatants prior to cryo-EM analysis. Shown are representative images of CA mutants with two magnifications. At least 200 particles were imaged per mutant. Black scale bars, 1 um; white scale bars, 100 nm.

776 **Figure 7**

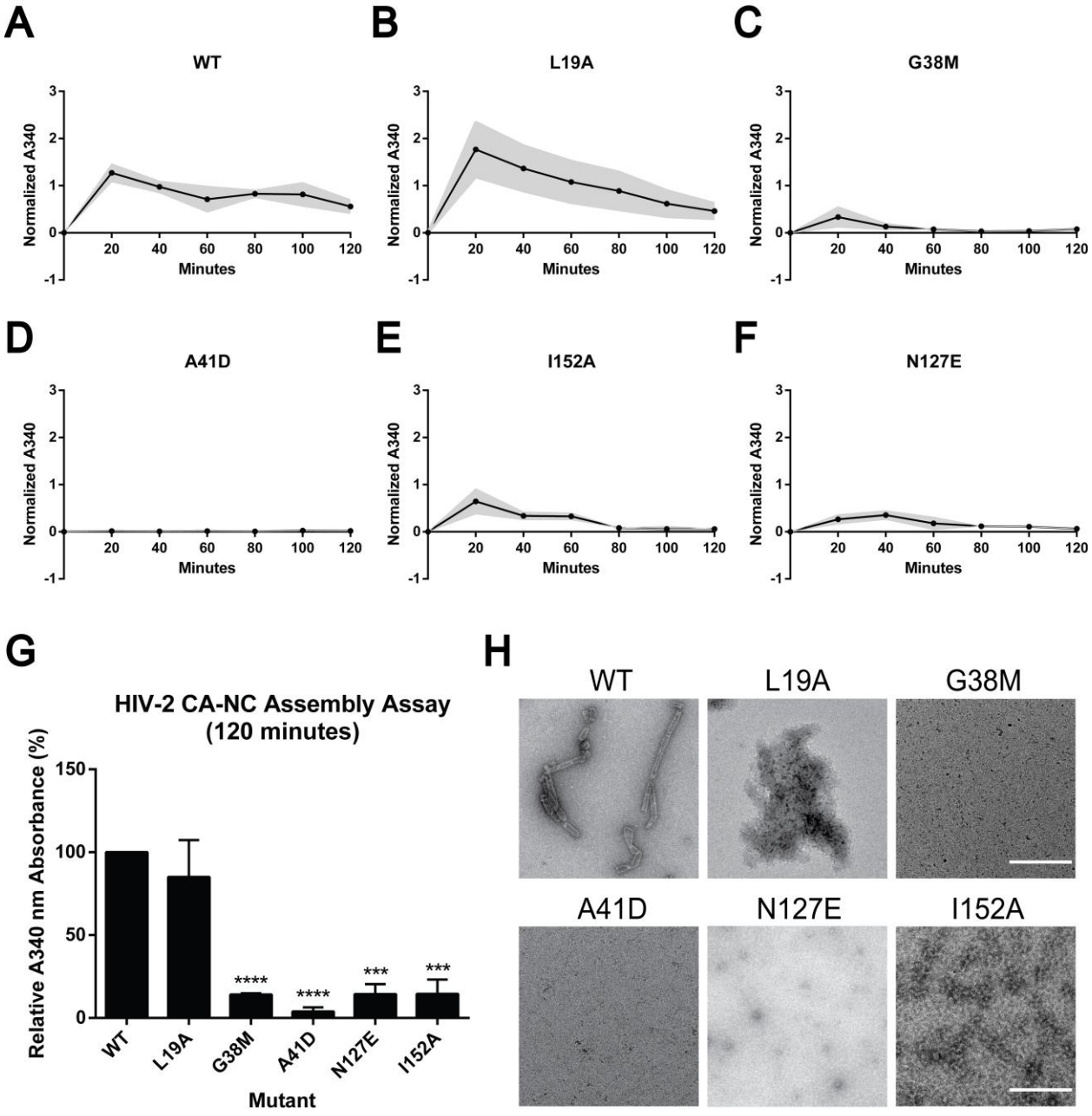

777
778

779 **Figure 7. *In vitro* HIV-2 CA-NC assembly analysis.** (A-F) Assembly kinetics of HIV-2 WT and
780 selected mutants were monitored by measuring light scattering at 340 nm while dialyzing the
781 reaction from sizing buffer into the assembly buffer at the indicated times. Readings were taken
782 every 20 minutes for 2 hours and corrected for any changes in reaction volume due to dialysis.
783 The grey area represents average ± standard error of the mean from three independent
784 experiments. (G) Relative A340 nm absorbance of selected HIV-2 CA mutants to WT, sampled
785 at 120 minutes. Error bars represent standard error of the mean from three independent
786 experiments. Significance relative to WT was determined by unpaired t test. ****, $P < 0.0001$; ***,
787 $P < 0.001$. (H) Negative staining EM images of assembly products, sampled at 120 minutes.
788 Scale bar, 500 nm.